Force Trigged Self-destructive Hydrogels

*Tharindu Rajasooriya,[1] Hiroaki Ogasawara,[2] Yixiao Dong,[2] Joseph Nicholas Mancuso,[2] and Khalid Salaita[2,3]**

Tharindu Rajasooriya

Department of Physics, Emory University, 400 Dowman Dr, Atlanta, GA, 30322, USA

Hiroaki Ogasawara, Yixiao Dong, Joseph Nicholas Mancuso, and Khalid Salaita

Department of Chemistry, Emory University, Atlanta, GA, 30322 USA

E-mail: k.salaita@emory.edu

Khalid Salaita

Wallance H. Coulter Department of Biomedical Engineering, Georgia Institute of Technology and Emory University, Atlanta, GA, 30322 USA

Keywords: CRISPR Cas12a, DNA hairpins, Self-destructive, Rheology, Responsive hydrogels, Mechanically induced depolymerization

Abstract:

This article has been accepted for publication and undergone full peer review but has not been through the copyediting, typesetting, pagination and proofreading process, which may lead to differences between this version and the Version of Record. Please cite this article as doi: 10.1002/adma.202305544.

Self-Destructive Polymers (SDPs) are defined as a class of smart polymers that autonomously degrade upon experiencing an external trigger, such as a chemical cue or optical excitation. Because SDPs release the materials trapped inside the network upon degradation, they have potential applications in drug delivery and analytical sensing. However, to the best of our knowledge, SDPs that respond to external mechanical forces have not been reported, as it is fundamentally challenging to create mechano-sensitivity in general and especially so for force levels below those required for classical force-induced bond scission. To address this challenge, we describe the development of force-triggered SDPs comprised of DNA crosslinked hydrogels doped with nucleases. Externally-applied piconewton forces selectively expose enzymatic cleavage sites within the DNA crosslinks, resulting in rapid polymer self-degradation. We describe the synthesis, chemical and mechanical characterization of DNA crosslinked hydrogels, as well as the kinetics of force-triggered hydrolysis. As a proof-of-concept, we also demonstrate force-triggered and time-dependent rheological changes in the polymer as well as encapsulated nanoparticle release. Finally, we show that the kinetics of self-destruction can be tuned as a function of nuclease concentration, incubation time, and the thermodynamic stability of DNA crosslinkers.

1. Introduction

Self-Destructive Polymers (SDPs) are a type of smart material that autonomously degrades upon external triggering. Many of the reported SDPs contain cryptic domains that become vulnerable to cleavage upon exposure to cues,[1] such as nucleophiles,[2] pH,[3] redox reaction,[4] enzymes,[5] ions,[6] and optical excitation to drive bond cleavage.[7] Thus, the external stimuli initiate the self-disintegration of the polymer network at the molecular level. Because polymer degradation can result in the release of the material trapped inside the network, SDPs are desirable materials for drug delivery systems,[1b, 8] sensors,[9] and in biotechnology, more broadly.[10] Interestingly, although chemical reactions can be triggered by chemical, optical, or mechanical inputs, to the best of our knowledge, all SDPs are designed to respond to chemical and optical inputs rather than mechanical inputs. Of

particular relevance is the area of mechanobiology, where mechanical cues drive conformational changes in individual proteins as well as protein hydrogel networks such as the extracellular matrix.[11] Such unfolding transitions are driven by piconewton (pN) scale forces and result in exposing cryptic sites that lead to binding and triggering of biochemical signaling pathways.[12] Thus, creating force-responsivity at this pN scale in synthetic materials may expand the scope of SDP applications to include force-induced drug delivery systems and force sensors that are compatible with cells.[13] It is important to also distinguish pN force-triggered self-destruction from more classical force-induced polymer degradation where cavitation, ball-milling, or other forms of mechanical input are used to cleave covalent bonds using > nN to N magnitude forces.[14] For reference, typical C-C bonds have energies of ~300 kcal/mol which requires ~10 nN forces to drive bond scissure.[15] In contrast, pN forces applied a distance of ~7 nm is ~1 kcal/mol at the scale of H-bond energies.[16] Hence, designing materials that can self-degrade with pN force inputs is a fundamental design challenge.

Hydrogels are a class of polymers that contain a three-dimensional network of hydrophilic polymer chains and are used for a wide variety of applications, including biosensing, drug delivery, extracellular matrix mimics for tissue engineering, cell adhesion, immunotherapy, and cancer therapy.[17] Here we aimed to introduce DNA linkages into hydrogel networks to encode a force-triggered self-destructive response. This design was motivated because of the well-characterized force responsivity,[18] reactivity with enzymes,[5b, 19] and programmability of DNA.[20] To create a force-trigged SDP using the DNA-linked hydrogel, two primary elements are required. The first is a well-defined force-sensor domain that undergoes a structural transition that is controlled mechanically. The second key element is a selective degradation reaction that is exclusively activated by mechanically induced conformational change. To satisfy these two criteria, we used DNA hairpins as the force sensor element and CRISPR Cas12a nuclease as the selective degradation system that is activated when DNA hairpins are unfolded under mechanical strain. Our previous body of work has extensively validated DNA hairpins (HP) as pN scale molecular force sensors.[21] DNA HP unfold when 3' and 5' ends of the DNA HPs are pulled apart with an external force. At $F_{1/2}$, which is defined as the force that leads to a 50% probability of unfolding, the

mechanical work applied to the DNA HP is equal to the sum of the free energy of base-pair hybridization ($\Delta G_{unfolding}$) and free energy of nucleotide stretching ($\Delta G_{stretch}$).[18a] Further validating the rigor of this approach, Walther and colleagues showed that DNA HPs can be integrated in hydrogels to provide a readout of strain upon stretching a bulk polymer material.[22] Another inspiration for our design is prior work by Collins and colleagues showing that Cas12a is sufficiently robust to cleave ssDNA crosslinks within hydrogels.[19a] Indeed, Cas12a was reported to selectively cleave ssDNA with 17 turnovers s^{-1} with k_{cat}/K_m = 1.7 x 10^7 $s^{-1}M^{-1}$ with minimal cleavage of dsDNA lacking complementarity to the CRISPR RNA (crRNA).[23] Considering this selectivity, we thought that CRISPR-Cas12a would be well-suited to create a force-triggered SDP.

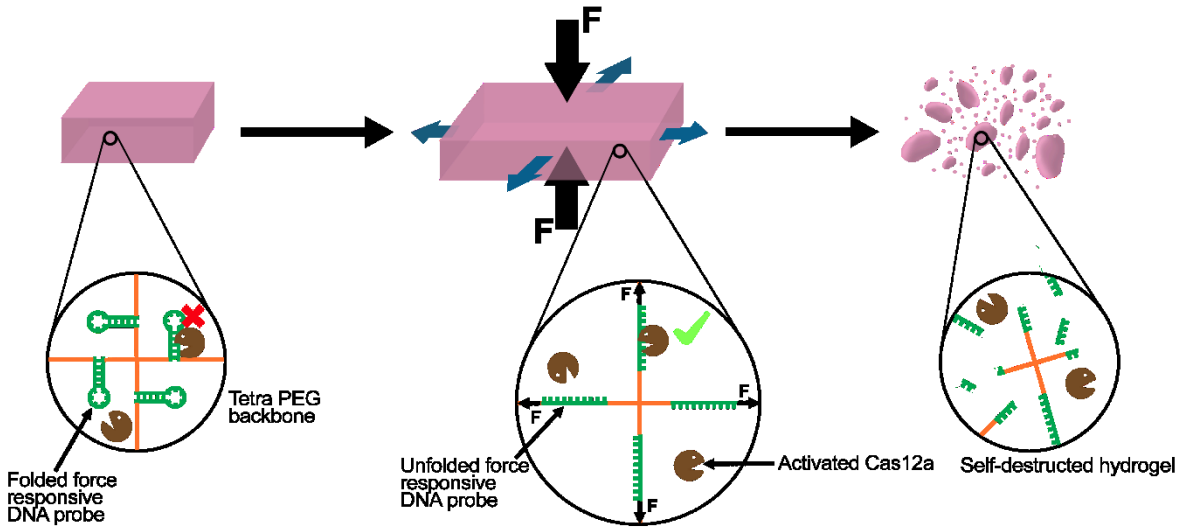

Scheme 1. Schematic of the force-triggered self-destructive hydrogel. The hydrogel composed of force-responsive DNA crosslinks and tetra PEG as the backbone polymer. (Left) DNA HPs are resistant to cleavage. (Middle) Force-induced opening of DNA HP sites leads to CRISPR-Cas12a cleavage of the DNA. Black and blue arrows indicate the external force and the force experienced by polymer backbone, respectively. (Right) This cleavage of ssDNA crosslinks triggers the self-destruction of the hydrogel.

We designed our force-responsive SDPs as shown in **Scheme 1**, where the tetra PEG (tPEG) hydrogel is crosslinked using force-responsive DNA HPs that remain folded at equilibrium in the absence of external force. When the force experienced by DNA HPs exceeds the $F_{1/2}$, DNA HPs unfold, and the cryptic Cas12a-vulnerable ssDNA sites become exposed. Because of this conformational change, Cas12a actively cleaves the ssDNA sites, leading to the breakage of the crosslinks and ultimately hydrogel self-destruction. To realize this design, we first screened a library of chemically-modified HPs to identify properties that would minimize the background cleavage. Next, we synthesized and characterized hydrogels that were formed by crosslinking tPEG DBCO with bisazide-modified DNA. We characterized force-triggered self-destruction of the hydrogel by measuring the degradation in response to external force firstly by applying a static force and then secondly by applying dynamic force using rheology. In both approaches, it was observed that hydrogels containing force-sensitive DNA HPs showed selective degradation under externally applied force and the hydrogel degradation highly depends on the enzyme concentration, incubation time, and the DNA sequence for the crosslinker.

2. Results and Discussion

To create force-triggered SDPs, it was important that we identify DNA structures that display minimal degradation in the absence of force but yet remain responsive to Cas12a cleavage upon mechanical unfolding. The ratio between k_{cat} ($F>F_{1/2}$) to k_{cat} (F=0) represents the signal-to-noise (S/N) ratio of the force-triggered SDP system and should be maximized as it dictates the quality of the responsive hydrogel. We first evaluated the stability of DNA structures at rest states (F=0) by using polyacrylamide gel electrophoresis (PAGE) (**Figure (1A)** top right). As shown in the **Figure (1B)** i-iv, four different types of DNA structures were tested, and these included (i) ssDNA, (ii) dsDNA, (iii) DNA HP, and (iv) “locked” DNA HP. The cleavage rate of ssDNA provides an indication of the maximum rate of Cas12a hydrolysis whereas the dsDNA provides the greatest Cas12a resistance when F=0 pN.

Unsurprisingly, ssDNA showed the greatest hydrolysis kinetics compared to the other three crosslinkers (**Figure (1C)** and **(D)**). In contrast to our expectations, DNA HPs hybridized with the locking strand (T-shaped HP) exhibited more rapid cleavage compared to the DNA HP. This is likely due to strain at the 3-way junction as confirmed by NUPACK analysis (Figure S1). Thus, we decided to further refine the DNA HP structure and avoid the T-shaped design. DNA HPs showed greater degradation compared to that of dsDNA, likely due to the single-stranded loop domain in the DNA HP, which is consistent with prior work by Rossetti et al.[25] To further confirm the cleavage site, we analyzed the cleaved products using denaturing PAGE. We found that hydrolysis was preferred at the stem-loop junction, and PAGE showed that the HP was mainly cleaved into two ssDNA fragments regardless of the nucleobase composition of the HP (Figure S2). To minimize this undesired cleavage of the HP (leakage reaction), we replaced the loop domain with two different sized PEG loops (PEG_6 and $(PEG_6)_2$) and introduced two phosphorothioate (PS) modifications at the base of PEG loop connecting the dsDNA stem (Figure 1(B), v-ix).

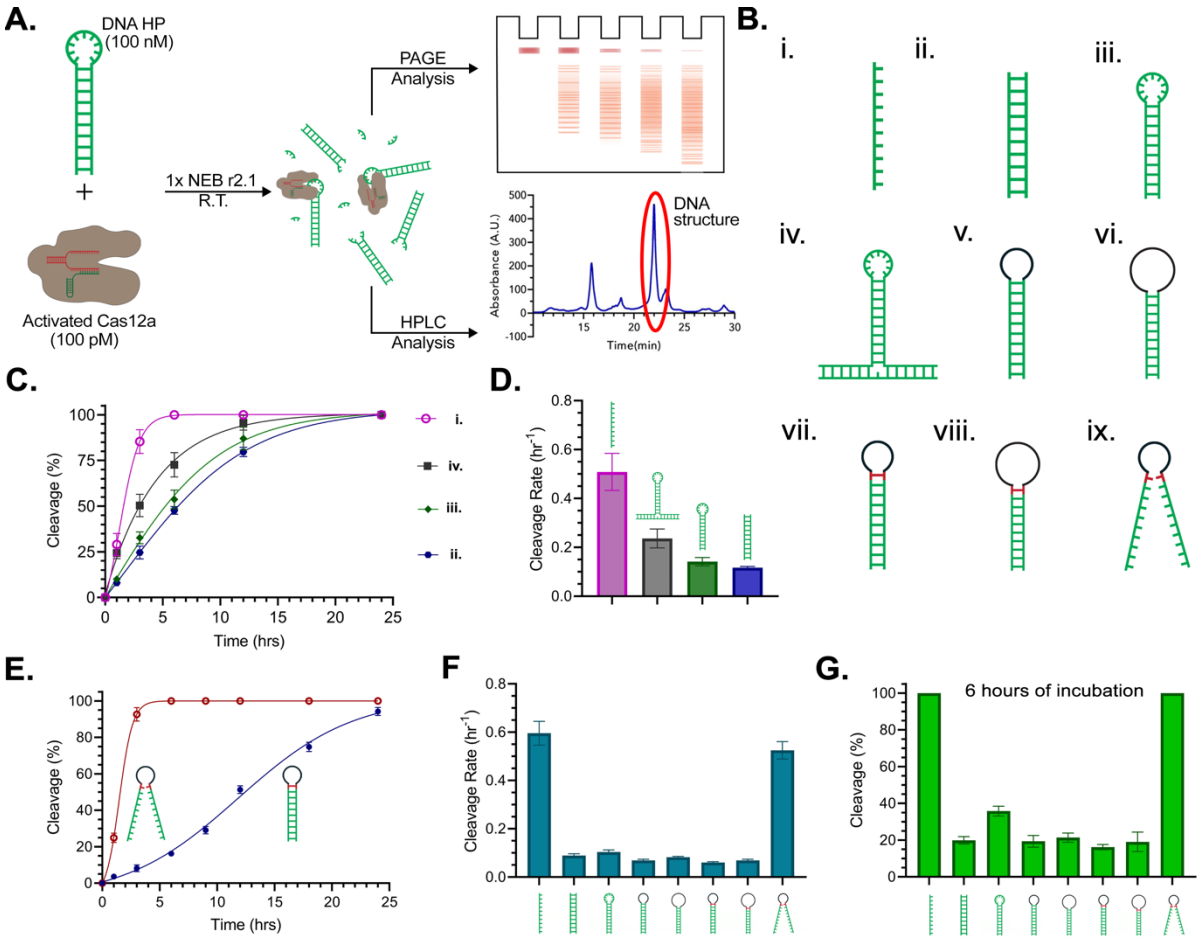

Figure 1: Optimization process conducted to find the best crosslinker for the force-triggered SDP hydrogel. (A) Quantification of the Cas12a activity on the DNA crosslinkers. First, DNA crosslinker was annealed and mixed with activated Cas12a enzyme for various time points, and then analyzed with PAGE over different incubation times (top) or with HPLC at indicated time points (bottom). The respective HPLC chromatogram for dsDNA is shown. For the PAGE analysis, the intensity of the DNA crosslinker was compared at different time points with the lane without Cas12a. For the HPLC analysis, before mixing of the Cas12a enzyme, the peak corresponding to the DNA structure shows larger area under the peak compared to after mixing with the Cas12a enzyme. (B) DNA structures used for the optimizations. (i) ssDNA (ii) dsDNA (iii) DNA HP (iv) locked DNA HP (v) dsDNA with PEG_6 spacer (vi) dsDNA with $(PEG_6)_2$ spacer (vii) dsDNA with PEG_6 spacer with PS modifications at the base of loop (viii) dsDNA with $(PEG_6)_2$ spacer with PS modifications at the base of loop (ix) ssDNA linked by PEG spacer with PS modifications at the connection of ssDNA and PEG

spacer. (C) Plot of the time-dependent Cas12a cleavage of the DNA structures (i-iv) in 1X NEB r2.1 buffer at room temperature evaluated by PAGE (D) Bar graph of Cas12a cleavage rates for DNA structures (i-iv) in NEB r2.1 buffer at room temperature calculated from time-dependent cleavage plot (Figure 1C). (E) Plot of the time-dependent Cas12a cleavage of the DNA structures (vii and ix as folded and unfolded DNA HP models, respectively) in 1X NEB r2.1 buffer at room temperature quantified by HPLC chromatograms. (F) Bar graph of Cas12a cleavage rates for DNA structures (v-ix) in NEB r2.1 buffer at room temperature calculated from time-dependent cleavage measurement quantified by HPLC chromatograms. (G) Bar graph of Cas12a cleavage (%) of DNA structures (v-ix) in NEB r2.1 buffer at room temperature at 6 hr time point. DNA crosslinker cleavage experiment for each structure was triplicated, and the error bars represent mean ± SD.

Due to the qualitative nature of PAGE, we next decided to perform HPLC analysis of DNA structure cleavage efficiency. HPLC analysis of cleavage had several advantages over PAGE including greater reproducibility and increased automation of data collection. Because of the automation, samples can be injected from the same reaction mixture at different time points leading to minimizing error associated with PAGE. Moreover, samples could be automatically injected into the HPLC in a precise time sequence, and using the heated column, the reaction was concurrently quenched which further improved time precision of the assay. Eight different DNA structures (i-iii, v-ix) as illustrated in the Figure 1(B) were tested to identify the optimum DNA crosslinker. The automated injection was performed after 1, 3, 6, 9, 12, 18, and 24 hrs. The integrated area under the peak in the chromatogram at 260 nm of the reaction mixture provided a quantitative readout of the trans cleavage activity of the Cas12a enzyme. The amount of intact DNA (highlighted in circles in Figure 1A) decreased over time due to enzyme cleavage (**Figure 1(E)**). It was also observed that the amount of intact activator dsDNA decreased over time due to cis cleavage activity of the enzyme. By normalizing the area under the peak for samples treated with Cas12a to that of samples lacking Cas12a, we were able to quantify the extent of hydrolysis and the cleavage rate (k_{obs}) (**Figure 1(F)** and S3). Furthermore, to compare the DNA structure cleavage over the 8 structures, we plotted the DNA cleavage efficiency at 6 hrs of incubation (**Figure 1(G)**).

As expected, ssDNA displayed the greatest cleavage rate (k_{obs}) when treated with Cas12a compared to the panel of tested DNA structures. dsDNA and DNA HPs showed more resistance to Cas12a cleavage compared to that of ssDNA. The greater enzyme activity against DNA HPs compared to that of dsDNA is likely due to cleavage of the ssDNA loop of the HP, which is consistent with the PAGE data (Figure 1(C) and (D)). Next, we found that the PEG loop significantly increased Cas12a resistance compared to that of conventional all-DNA HPs (Figure 1F). The introduction of PS linkages along with the PEG_6 loop showed 16.2 ± 1.0% cleavage after 6 hrs of incubation. In contrast, all DNA HP showed 36.7 ± 2.8% cleavage at the same time point, thus indicating that these chemical modifications half the leakage of the assay. This increase in Cas12a resistance agrees with the PAGE data, which showed preferential cleavage at the base of the loop in all DNA HP (Figure S2). As noted above, we tested two different sizes of PEG loops as the length may affect the duplex stability at the base of loop structure and thus the stability against Cas12a cleavage. As shown in Figure 1F, the difference in the cleavage rate (k_{obs}) of PEG_6 and $(PEG_6)_2$ is insignificant, suggesting that both linker offers sufficient flexibility to stabilize the stem-loop structure avoiding cleavage at the nucleotides proximal to the loop. PS modified HP with PEG_6 and $(PEG_6)_2$ loop showed k_{obs} = 0.060 ± 0.002 hr^{-1} and 0.066 ± 0.004 hr^{-1}, respectively. Considering these observations, we choose the DNA HP design integrating PS modifications at the junction with an internal PEG_6 loop as the DNA crosslinker for the SDP as this afforded a ~ 5 fold differential in Cas12a cleavage rate when comparing the HP to the unstructured linear DNA. Future optimization using locked nucleic acids and other chemical modification may further enhance this differential.

We next aimed to generate hydrogels that integrate this optimized force-responsive DNA HP as the crosslinkers. We first evaluated different types of DNA-linked hydrogels and decided to employ PEG-based polymers because of their greater stretchability and biocompatibility compared to that of polyacrylamide hydrogels.[26] We specifically crosslinked the DNA HP with tetra-PEG (tPEG) macromolecules because 4-arm PRG has been shown to generate robust covalently crosslinked networks with DNA.[27] Our initial work to generate hydrogels by coupling tPEG with activated NHS-esters to bisamine-modified DNA were unsuccessful (Figure S4). This was consistent with the work done by Crusen et al, where they showed that a >64-fold excess of the NHS-ester is required to achieve quantitative conversion of amine

groups on DNA due to the instability of the activated ester in the aqueous medium.[22a] Inspired by Zheng et al.'s recent report, we then used the strain-promoted azide-cyclooctyne click reaction between tPEG-DBCO and bisazide-functionalized DNA.[28] tPEG-DBCO was synthesized by NHS reaction as illustrated in **Figure 2(A)** and purified using HPLC (Figure S5(A)). The degree of DBCO-functionalization (DOF) of the tPEG macromolecule was evaluated by the absorbance at 307 nm of the conjugated DBCO (DOF = 3.77 ± 0.13) which showed a fairly pure monomer following purification (Figure S5(B)). Note that tPEG-DBCO degrades slowly in solution and the partially degraded tPEG DBCO can significantly affect the crosslinking density and thus storage modulus (G') (Figure S6). Therefore, after synthesis, the product was lyophilized, aliquoted, and stored at –80 °C until needed. Azide-modified DNA crosslinkers were synthesized as shown in **Figure 2(B)**. The formation of the bisazide modified DNA crosslinker was confirmed using ESI mass spectrometry (Figure S7).

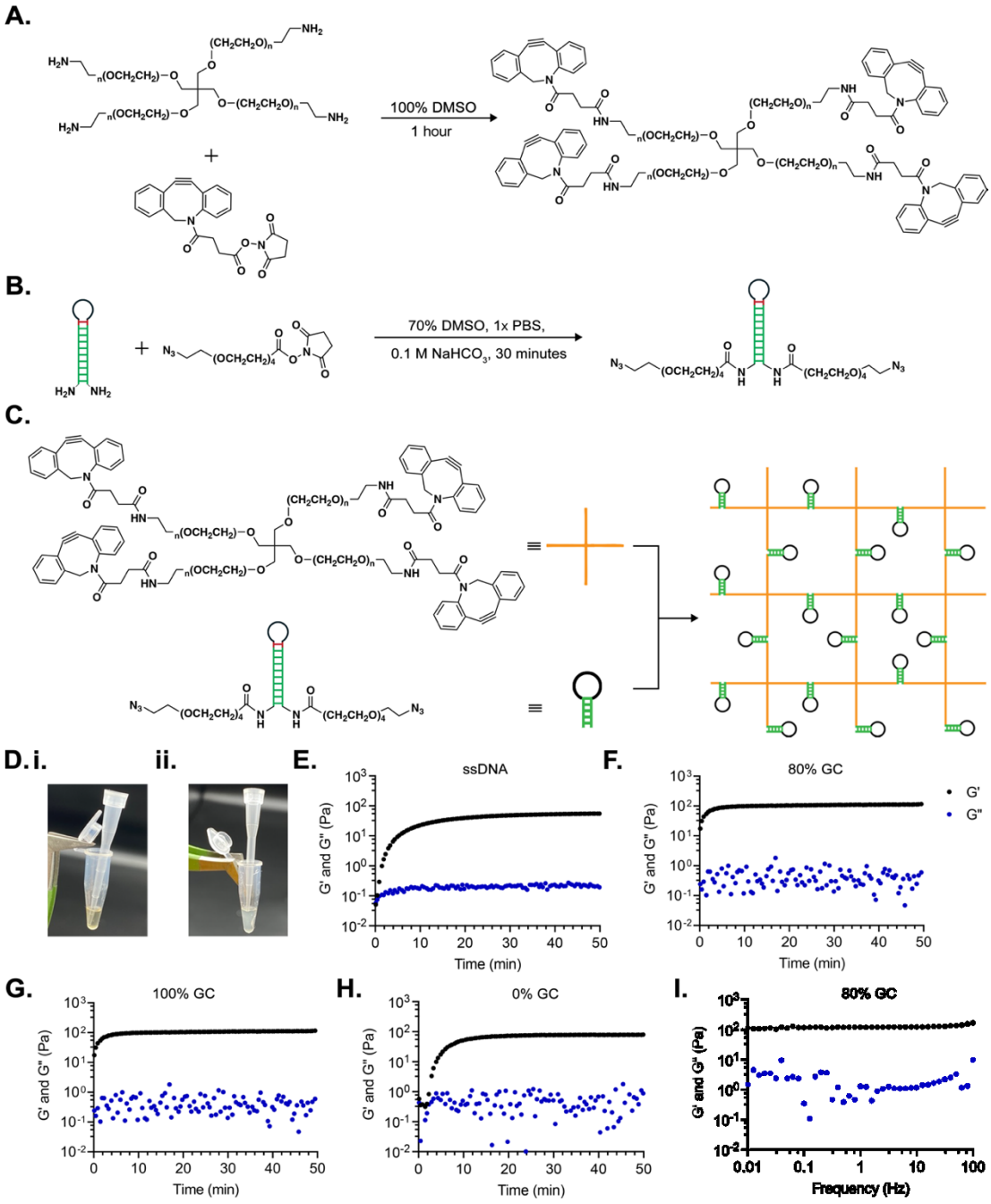

Figure 2: Synthesis and characterization of the force-responsive DNA crosslinked tetra PEG hydrogel. (A) Synthesis of tetra PEG DBCO. The synthesis was conducted in anhydrous DMSO by mixing tetra PEG amine (Mw = 10k g mol^{-1}, n= ~57) and DBCO NHS ester, and the final product was purified by reversed-phase HPLC. (B) Synthesis of bisazide-modified DNA crosslinkers. The synthesis was conducted by mixing

diamine-modified DNA crosslinkers with azido PEG_4 NHS ester at 70% DMSO, 1x PBS and 0.1 M $NaHCO_3$ for 30 mins. The product was purified by HPLC. (C) DNA crosslinked hydrogel was synthesized by crosslinking 2.5 mM tPEG DBCO and 5.0 mM bisazide-modified DNA. The crosslinking reaction was conducted in 1x NEB r2.1 buffer with an equal ratio between DBCO and azide functional groups. (D) Photographs of the DNA crosslinked hydrogel to confirm the hydrogel formation. (i) With the absence of the DNA crosslinker, no hydrogel formed and the 10 µL pipette tip sank to bottom. (ii) With the presence of the DNA crosslinker, hydrogel was formed, and the pipette tip was remained on the top of the hydrogel, confirming the formation of the hydrogel. (E) Representative plot of time-dependent measurement of storage modulus (G') and loss modulus (G'') after mixing the 2.5 mM tPEG-DBCO and 5.0 mM bis-azide-modified ssDNA crosslinkers in 1x NEB r2.1 buffer. (F) Representative plot of time-dependent measurement of G' and G'' of the DNA HP (80% GC) crosslinked hydrogel. Rapid hydrogel formation was observed, and, within 5 min, the storage modulus of the hydrogel reached a plateau of around 100 Pa. (G) Representative plot of time-dependent measurement of G' and G'' of the 100% GC content HP crosslinked hydrogel. (H) Representative plot of time-dependent measurement of G' and G'' of the 0% GC content HP crosslinked hydrogel. (I) Representative plot of the storage modulus (G') and loss modulus (G'') of the DNA HP (80% GC) crosslinked hydrogel at different rheometer frequency to test the stability of hydrogel. For the observed frequency range, the hydrogels kept their gel structure as the G' were larger than G''.

Two types of hydrogels were synthesized by mixing 2.5 mM tPEG-DBCO with 5.0 mM bisazide DNA HP crosslinker or ssDNA in NEB r2.1 buffer. Both DNA crosslinkers were of identical length and comprised of 30 nucleotides with a 6 ethylene glycol linker inserted in the middle. The ssDNA crosslinker simply scrambled one arm of the stem to denature the parent HP crosslinker. Qualitatively, the formation of the DNA HP hydrogel was confirmed using a pipette tip as shown in the photographs in **Figure 2(D)**. Withholding the DNA HP crosslinker led the tip to sink to the bottom of the tube; in contrast, the sample containing both DNA HP crosslinker and tPEG formed a gel, which prevented the tip from sinking. Quantitative characterization of the mechanical properties of the DNA HP gel was performed using rheology (**Figure 2(E) – (I)**). In the time sweep experiment, we mixed the two precursors and then immediately started recording G' and G" using a parallel-plate rheometer (see methods). The time sweep data showed that the gelation kinetics were rapid, and the crossover point of G' and G" was not observed likely because the hydrogel formed during the ~1 min deadtime between mixing of the precursors and initiating data collection. As shown in Figure I(E)-(F), it was observed that gels synthesized from linear ssDNA

crosslinkers were significantly softer (G'_{max} = 63.7 ± 11.0 Pa at *t* = 50 min) compared to identically prepared hydrogels employing the DNA HPs (G'_{max} = 107.3 ± 6.2 Pa at *t* = 50 min). Previous work has shown that hydrogel stiffness is directly related to the chain length of the crosslinkers.[29] Although the ssDNA and HP crosslinkers have the same contour length (~24 nm), the equilibrium length of the hairpin crosslinks is effectively the width of the DNA duplex (~2 nm) which is significantly smaller than the estimated mean end-to-end length of the ssDNA (~5-7 nm). Accordingly, the hydrogel crosslinked with HPs showed 2-fold greater stiffness. Because the molecular scale structure of DNA changes the macroscale hydrogel stiffness, we wondered whether the molecular scale DNA HP stability affect the macroscale mechanical properties of the DNA-linked hydrogel. To test this hypothesis, we used two other DNA HP's with 100% and 0% GC content to synthesize the hydrogels. As shown in the Figure 2 (G) – (H), it was observed that, when the 100% GC content HP is used, the stiffness of the hydrogel was increased to 200.0 ± 21.3 Pa. In contrast, when the 0% GC content HP is used, the stiffness of the hydrogel decreased to 67.5 ± 14.8 Pa. These results indicate that the macroscale stiffness of the hydrogel reflects the molecular scale HP stability, which can be tuned by GC content of the DNA HP. The frequency sweep shows the stability of the hydrogel over the tested frequency range of 0.01 – 100 Hz (Figure 2(I)) and exhibits classic hydrogel behavior.

We next focused on demonstrating force-induced hydrogel degradation. As illustrated in **Figure 3(A)**, hydrogels were sandwiched between two glass slides to apply compressive forces that stretch the polymer network. This was achieved by forming the hydrogel in between two hydrophobic glass slides that were pre-treated with a 2% solution of dimethyldichlorosilane and pressed to spread the gel into a thin film. Note that functionalizing the glass surface with dimethyldichlorosilane was critical to reduce hydrogel adhesion to the substrate (Figure S8). Subsequently, we aimed to measure and maximize the applied strain to the hydrogel. A 200 μm spacer was introduced between the glass slides, and then the strain was quantified by measuring the hydrogel 2D area before and after sandwiching with the second glass slide (Figure S9 and S10). We next investigated the optimal volume of the hydrogel for a 200 μm spacer by tuning the total amount of material and measuring the strain. As shown in Figure S9, we found that ~30 μL volume offered maximal strain which was used in all subsequent measurements. To determine the reproducibility of the strain

measurement, we next quantified the hysteresis in deformation of the hydrogel after five cycles of compression and relaxation (Figure S10). We found that the hysteresis was insignificant (<5% change) regardless of whether radial or area strain was quantified. Unsurprisingly, the smaller hydrogel volumes produced greater hysteresis. Considering these data, we identified 30 µL as the optimum volume for testing force-induced destruction experiments in our experimental setup while also conserving reagents. Note that this optimal volume was empirically determined and is specific for our experimental setup using a 200 µm thick spacer between the slides.

To detect hydrogel destruction, we doped in 100 nm diameter gold nanoparticles (AuNP) that were stabilized using 5,000 g/mol Mw PEG_n-SH and trapped within the network. Without the Cas12a in the hydrogel, the introduction of an external mechanical force did not induce hydrogel degradation (**Figure 3(B(i)**). This was confirmed by observing that the AuNPs remain bound within the gel, confirming that the gel remained intact. To test hydrogel self-destruction, we introduced Cas12a enzyme, which preferably cleaves DNA crosslinker when it is extended under force, to the precursor solution before the gelation. When the Cas12a enzyme was introduced and the gel was allowed to incubate at zero force for 3 hrs at 37 ºC, we did not observe full self-destruction of the hydrogel (**Figure 3(B (ii)**). However, even without the application of external force, we observed slow hydrogel self-destruction after 6 hrs of incubation at 37 °C. The slow self-destruction of the hydrogel in the absence of external force suggests leakage of the assay which is likely due to dynamic breathing, or transient unfolding, of the DNA HP. Such, unfolding events are due to thermal fluctuations.[30] For example, the unfolding rate for a DNA hairpin with 22% GC content is 1.5×10^{-2} s^{-1} at 45 ºC and zero force and this value exponentially grows as a function of applied force.[31] To confirm this, we tested Cas12a activity on hydrogels synthesized using DNA HPs with different GC content (Figure S11). While the hydrogels crosslinked with ssDNA and 0% GC DNA HP show complete self-destruction 30 minutes, both hydrogels crosslinked with 80% and 100% GC DNA HP show resistance to the Cas12a activity under zero external force. More importantly, compared to the 80% GC DNA HP crosslinked hydrogel, 100% GC DNA HP crosslinked hydrogel shows 17% less AuNP release to the buffer at 3 hrs. This indicates that thermal breathing of the DNA HP contributes to self-destruction of DNA HP crosslinked hydrogels. In contrast, with the introduction of both Cas12a and external force, it was

observed near complete AuNP release supporting self-destruction of the hydrogel after 3 hrs of incubation at 37 °C (**Figure 3(B(iii)**). This force-induced self-destruction validates our hypothesis that external force application to the hydrogel induces the opening of the DNA HP crosslinkers inside the hydrogel, triggering Cas12a cleavage of DNA crosslinker, ultimately leading to hydrogel self-destruction.

To quantify the self-destruction of the hydrogel, we measured the amount of AuNP release to the buffer by the absorbance at 535 nm using a UV-Vis spectrometer. As shown in **Figure 3(C)**, we tested three different hydrogels for force-induced self-destruction. The hydrogels are composed of tPEG-DBCO and three different crosslinkers, including tPEG-azide (no self-destruction control: bisPEG-tPEG hydrogel), linear ssDNA (self-destruction control: ssDNA hydrogel), and force-responsive DNA hairpin (HP hydrogel). The AuNPs inside non-self-destructive bisPEG-tPEG hydrogel did not diffuse into the buffer solution regardless of the presence of external force and Cas12a. In contrast, AuNPs trapped within ssDNA hydrogels were released into solution when Cas12a is present, regardless to the application of external force. Another notable observation was that ssDNA hydrogel degradation without force was more rapid (30 min) compared to the hydrogel degradation with force (2 hrs). This may be due to the decreased binding probability of Cas12a enzyme to stretched ssDNA under the external force.[32] When the external force is absent, the HP hydrogel shows a significantly lower self-destruction rate compared with ssDNA hydrogel, while, when the external force is applied, HP hydrogel shows a comparable self-destruction rate with that of the ssDNA hydrogel. This difference between the presence and absence of external force indicates that the DNA HP opening induced by external force exposes cryptic ssDNA sites which can be cleaved by Cas12a. To quantify the rate of force-triggered self-destruction, we recorded the hydrogel self-destruction in the presence or absence of external force and Cas12a enzyme (8 μM and 0.8 μM) at each time point (Figure S12). Notably, while the self-destruction kinetics was slowed by decreasing the Cas12a concentration, the undesired self-destruction without the external force was greatly suppressed when the 0.8 μM Cas12a was used. Although we used 8 μM enzyme concentration for the rheometer experiments due to time constraints, lowering enzyme concentration promises improved external-force selective SDP response.

Force-induced hydrogel degradation was also validated using rheology measurements. Specifically, time-dependent stress relaxation of ssDNA, 80% GC content HP, and 100% GC content HP crosslinked hydrogels with and without Cas12a enzyme were performed to quantify the force induced hydrogel self-destruction (**Figure 3(D)** and Figure S13A). When Cas12a is absent, the stress in the hydrogel decays in a constant manner and reaches its plateau at approximately 15% of the maximum load regardless of the crosslinker used (**Figure 3 (D (i)**). In contrast, when the Cas12a enzyme is present, the measured force applied to the hydrogels initially follows a slow and constant decay, but after a certain time point, the measured force suddenly drops to zero. The initial relaxation is caused by the normal hydrogel relaxation behavior, while the sudden drop in stress is the result of Cas12a self-destruction of the gel (**Figure 3(D (ii))**). This sudden change in the polymer stress may be due to the relatively larger hydrodynamic diameter of Cas12a protein (~19 nm) preventing its diffusion inside the smaller pore sizes of the PEG polymer network (~6 nm for Mw = 10k g mol^{-1} PEG)[29, 33] This hypothesis aligns with our observation that adding Cas12a enzyme to pre-synthesized DNA crosslinked hydrogels leads to significantly slowed hydrogel degradation kinetics compared to that of Cas12a doped *within* the hydrogel. The hindered rate of gel degradation is likely due to slow diffusion of Cas12a within the hydrogel. We postulate that the abrupt drop in gel stress may occur once sufficient local degradation of the hydrogel leads to release of entrapped Cas12a, accelerating the rate of gel hydrolysis.

For better comparison between the gels that included Cas12a and those without Cas12a, we normalized the polymer stress (normal force) and overlayed the force relaxation curves of the hydrogel synthesized with 80% GC content HP (Figure S13B). In the absence of Cas12a, the gel showed slower initial relaxation rates compared to that of the same hydrogel containing Cas12a enzyme. This difference in initial relaxation rates suggests that, while there is no acute force drop, Cas12a cleaves the polymer network continuously during the application of external force which leads to a decrease in hydrogel elasticity over time. Note that the two-phase decay and stretched-exponential functions are often used to quantitatively evaluate such decay curves;[34] however, past models were developed for static,[34] stably crosslinked hydrogels, not for dynamically changing hydrogels. Thus, we only evaluated the relaxation rates qualitatively.

We next compared the force relaxation plots for gels synthesized using ssDNA and 80% and 100% GC content HPs (Figure 3D (ii)). We found complete loss of stress at ~50, ~65, and ~80 min, for the ssDNA, 80% GC HP and 100% GC HP, respectively, indicating that the molecular stability of the HP dictates its response to macroscopic forces and associated force-triggered destruction. The normal force of ssDNA crosslinked hydrogel (~1.0 N) was much lower than the other gels (~1.6 N). This could be due to the Cas12a cleavage of ssDNA during the gelation before applying the external force, resulting in the failure of capturing the fully crosslinked hydrogel. As described earlier, we normalized the normal force to each maximum force for 80% and 100% GC HP crosslinked hydrogels (Figure S13C). Interestingly, 80% GC HP crosslinked hydrogel showed much faster initial relaxation compared with that of 100% GC HP crosslinked hydrogel. This reflects the thermodynamic stability of HP folding where higher GC content leads to more stable folding conformation, which protects the crosslinkers from Cas12a cleavage. This result indicates that, similar to the storage modulus (G') measurements, the molecular scale HP stability dictates the bulk material properties.

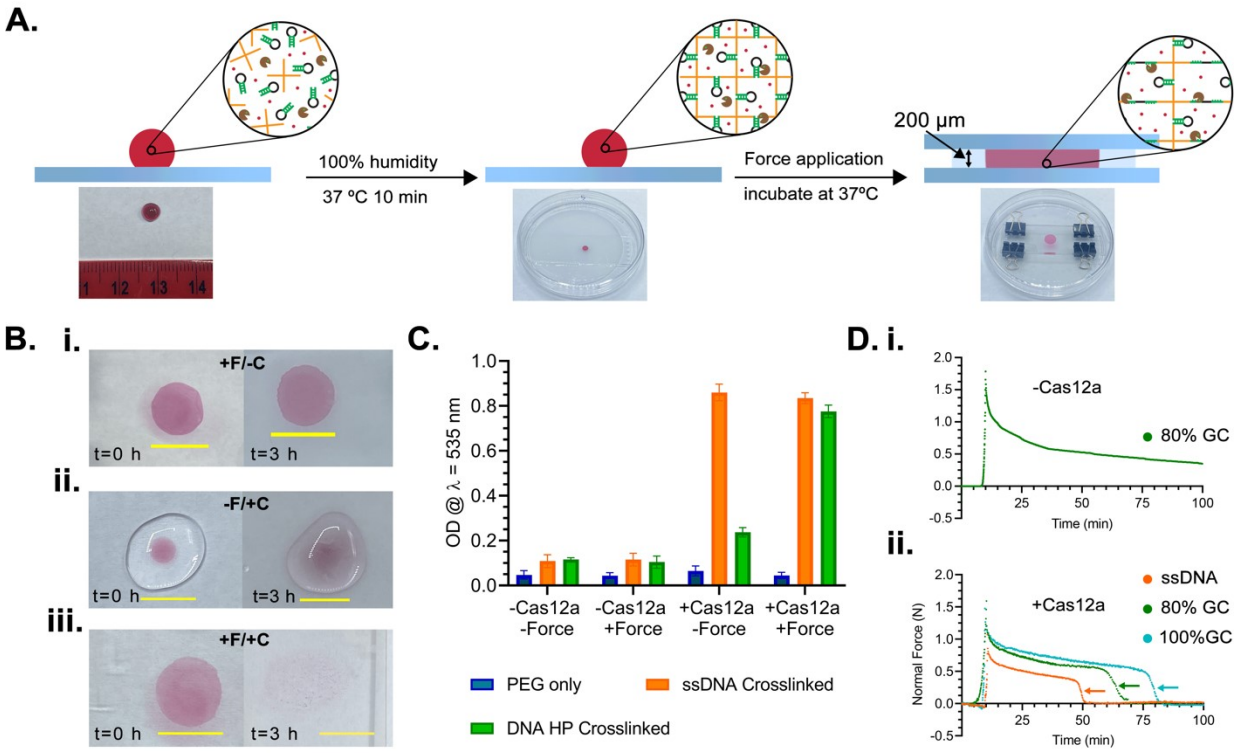

Figure 3: Demonstration and optimization of the force-triggered self-destruction of the DNA crosslinked hydrogel. (A) Illustration of the force application experiment to the DNA HP crosslinked hydrogel. (left) The hydrogel precursor solution was mixed with the activated Cas12a and placed on top of a hydrophobic glass slide. (middle) Then, it was incubated in a closed wet petri dish for 10 minutes at 37 ºC to complete the gelation. (right) The formed hydrogel was sandwiched with two glass slides. Inside the sandwiched glass slides, we introduced the 200 µm spacer to obtain reproducible thickness and buffer was added to avoid dryness. Force was applied to the hydrogel by clipping the glass slides in a wet petri dish to maintain 100% humid condition. (B) Photographs of DNA HP crosslinked hydrogels under different conditions (scale bar = 1 cm) (i) The hydrogel prepared without the Cas12a under external force. The photographs were taken at t = 0 and 3 hrs of continuous external force application. (ii) hydrogel prepared with the Cas12a. The photographs were taken at t = 0 and 3 hrs of incubation without external force application. (iii) Force-responsive DNA HP crosslinked hydrogel prepared with the Cas12a. The photographs were taken at t = 0 and 3 hrs of incubation with the continuous external force application. (C) Bar graph showing the degradation of hydrogels under different conditions. Blue, orange, and green bars represent the hydrogels crosslinked by the tPEG-N_3 (10k), ssDNA, and 80% GC HP, respectively. Each condition was triplicated, and the error bars represent mean ± SD. (D) Representative plots of time courses of stress relaxation of the DNA HP crosslinked hydrogel (i) without the Cas12a enzyme and (ii) with the Cas12a enzyme. Orange, Green, and Cyan color represents the data acquired with ssDNA, 80% GC HP, and 100% GC HP crosslinked hydrogel. With the presence of the enzyme, the stress in the hydrogel showed a sudden decrease. This sudden decrease in stress (as indicated with arrows) is dependent on the GC content of the HP. ssDNA crosslinked hydrogel show the fastest degradation at ~ 50 minutes. DNA HP degraded at ~ 65 minutes. 100% GC HP crosslinked hydrogel showed the most resistance to Cas12a activity and showed degradation around 80 minutes.

3. Conclusion

In summary, we demonstrated a force-triggered self-destructive hydrogel crosslinked by force-responsive DNA hairpin structures. Application of an external force triggers degradation of the DNA crosslinkers and loss of integrity of the gel. We utilized HPLC chromatograms to quantify the DNA degradation upon Cas12a cleavage and identified the DNA HP crosslinker with the least Cas12a degradation when DNA HP is folded. Due to the Cas12a enzyme degrading the hairpin loop in the absence of mechanical force, we designed a DNA HP crosslinker with a PEG loop spacer and modified the two proximal

phosphodiester groups with nuclease-resistant phosphorothioate groups to minimize non-force-triggered cleavage. With the bis-azido modified DNA crosslinker and tPEG DBCO (10k), we synthesized the force-triggered self-destructive hydrogel. The force-triggered self-destruction was characterized by comparing the force-responsive DNA HP crosslinker and ssDNA crosslinker. We visualized the hydrogel self-destruction using gel-doped AuNPs and this was quantified using UV-Vis spectroscopy. Importantly, because DNA-coated AuNPs are widely used for gene regulation, sensing, as well as material assembly, we anticipate that force-triggered self-degradation of hydrogels and subsequent release of DNA-AuNPs system could find a broad range of further applications in the future.[35] This may include force-triggered AuNP drug release to disease sites where the cells exert unusually high traction forces or in regions of elevated shear flow, such that would be experienced in thrombotic occlusions.[36] Note that, for rapid SDP response, Cas12a needs to be incorporated within the gel as adding Cas12a after gel formation leads to significantly slower degradation rates, likely due to hindered diffusion (Figure S14). In some instances, it may be desirable to control the formation of SDP material by adding Cas12a externally which produces the SDP when Cas12a is introduced and added advantage of preserving the polymer integrity until the response function is needed. Furthermore, we have demonstrated that the force-triggered self-destruction of the hydrogel can be controlled by tuning the Cas12a enzyme concentration, incubation time, and GC content of the DNA HP crosslinker. One potential challenge in using this SDP material may be related to bottleneck in scaling up the synthesis of chemically modified nucleic acids. This may be the case currently, but recent analysis suggests that the cost of DNA synthesis continues to drop rapidly as a function of time due to increasing demand and improving procedures.[37]

Supporting Information

Supporting Information is available from the Wiley Online Library or from the author.

Acknowledgements

This work is supported by NIH RM1GM145394, NIH NIGMS 1R01GM131099, and NIH RO1AI172452. H.O. acknowledges the Naito Foundation and the Uehara Memorial Foundation for the research support. The authors would like to thank the Emory Mass Spectrometry Center and Dr. Fred Strobel for ESI-MS measurement, Mr. Pablo Illings and Dr. Eric Weeks for rheology measurements. Additionally, we thank Dr. Eric Weeks and Dr. Justin Burton for helpful discussions regarding the rheology data.

Conflict of Interest

The authors declare no conflict of interest.

Experimental/ Method section

Materials: All the DNA and RNA used in the study were purchased from Integrated DNA Technologies (IDT) and Horizon Discovery Biosciences Limited, respectively (Table S1). EnGen® Lba Cas12a (Cpf1) (M0653T) enzyme and the NEBuffer™ r2.1 buffer (10X, B6002S) were purchased from New England Biolabs (NEB). 30% Acrylamide/Bis Solution, 29:1 (1610156) was purchased from Bio-Rad Laboratories. Urea (9510-500GM) and *N,N,N',N'*-tetramethylethylene diamine (TEMED, T9281-25ML), ammonium persulphate (APS, A3678-100G), H_3BO_3 (B0394-500G), EDTA (EDS-500G), NaCl (S1679), anhydrous dimethyl sulfoxide (DMSO, MX1457-7), KCl (PX1405), $NaHCO_3$ (56014-500G), H_2SO_4 (SX-1244-6), H_2O_2 (30wt%, 216763-500ML), and AuNP (100 nm) in citrate buffer (742031-25ML) were purchased from Millipore Sigma. Diamond™ nucleic acid dye (H1181) was purchased from Promega. 10X TE buffer (10421) was purchased from Cepham Life Sciences. TetraPEG NH_2 (Mw = 10k g mol^{-1}, 4arm-PEG-NH2-10K-1g) was purchased from Laysan Bio Inc. DBCO NHS ester (A133-100) and azido-PEG_4-NHS ester (AZ103-1000) were purchased from Click Chemistry Tools. tPEG Azide (Mw = 10k g mol^{-1}, PSG-492) and

bisazide PEG (Mw = 600 g mol^{-1}, PSB-3241) were purchased from Creative PEG Works. 2.0 M TEAA buffer (60-4110-62) was purchased from Glen Research. 25 mm coverslips (round no. 2, 48382-085) were purchased from VWR. Plain Diamond® White Glass Microscope Slides (25×75 mm, 90º ground edges, plain, 1380-10) were purchased from Grobe™ Scientific. Repel-Silane ES (2% solution of dimethyldichlorosilane dissolved in octamethylcyclooctasilane, #17-1332-01) was purchased from GE Healthscienes, Cytiva. Thiolated PEG (Mw = 5000 g mol^{-1}, PG1-TH-5k) was purchased from NANOCS.

Instruments: Milli-Q grade water for all experiments was obtained from a Barnstead Nanopure water purifying system (Thermo Fisher Scientific) that indicated a resistivity of 18.2 MΩ. Oligonucleotide and modified tPEG DBCO purification were performed using a high-performance liquid chromatography (HPLC, Agilent 1200) equipped with a diode array detector. All the absorbance measurements were obtained using a Nanodrop 2000 UV-Vis Spectrophotometer (Thermo Fisher Scientific). Mass identification of the modified oligonucleotides was performed with ESI mass spectrometer (Thermo Fisher Scientific, Orbitrap). PAGE was performed using Mini-PROTEAN Tetra Cell (BIORAD). Gel imaging was performed using iBright gel imaging system (Thermo Fisher Scientific). AR2000ex rheometer (TA Instruments) was used to perform temperature controlled rheological tests. DNA hybridization was done using T100 Thermal Cycler (BIORAD).

DNA Hybridization: DNA oligonucleotides used in the study for gel electrophoresis and HPLC analysis were hybridized at 100 µM in a 0.2 mL PCR tube in 50 mM NaCl, 1X TE buffer. The solutions were heated to 95 °C for 5 min and then cooled at a rate of 2.5 °C per minute to 4 °C using the thermocycler. DNA HP crosslinkers used to synthesized hydrogels were hybridized at 5.0 mM with same procedure.

Polyacrylamide gel electrophoresis of Cas12a cleavage of DNA structures: 20% denaturing polyacrylamide gel was prepared by dissolving 7.2 g of urea in 10 mL of 30% Acrylamide/Bis

solution (29:1) and 1.5 mL of 10X TBE buffer (pH = 8.2). Next, the volume of the solution was adjusted to 15 mL with Milli-Q grade water. To this solution, 12 µL of TEMED and 50 µL of 30% APS solution were added and the solution was quickly transferred into a gel casting tray using 10 tooth comb. The oligonucleotide mixture with the Cas12a enzyme was prepared by mixing 10 µL of anneal solution of 100 µM DNA, 1 µL of 1 µM Lba Cas12a, 1 µL of 2 µM gRNA and 1 µL of 1 µM dsDNA activator and 86 µL of nanopure water. Before loading into the gel, from this mixture, 2 pmol of oligonucleotides were mixed with ethidium bromide (10 mg/mL). Then, the oligonucleotide solutions were loaded into each well of the gel and electrophorese for 120 minutes under 95 V potential. After the electrophoresis, the gel was stained with 10,000X Diamond™ nucleic acid dye (5 µL in 50 mL of 1X TBE buffer) for 10 minutes and imaged using iBright gel imaging system. Using the fluorescence intensity of oligonucleotide staining, the cleavage percentages were calculated according to equation 1, where, $P_C(t)$ is the percent cleavage of the DNA crosslinker at the given time (t hrs), $I(0)$ is the intensity of the corresponding band at t = 0 and $I(t)$ is the intensity of the corresponding band at t.

$$P_C(t) = \left[\frac{I(0)-I(t)}{I(t)}\right] \times 100 \qquad (1)$$

Next, the data were fitted to a single exponential in GraphPad Prism version 8.4.3 for Windows. To calculate the cleavage rate (k_{obs}), we used the nonlinear curve fitted value from the GraphPad Prism software. $P_C(t = 0)$ was set to 0, and $P_C(t=24)$ was set to 100%. The data was triplicated, and in each dataset, separated k_{obs} value was calculated and averaged.

HPLC analysis of Cas12a cleavage of DNA structures: Resistance to the Cas12a enzyme for each DNA probe was tested as follows. First, 300 µL solution of annealed DNA crosslinker with Cas12a enzyme was prepared in a 300 µL HPLC vial insert by mixing 30 µL of annealed solution of 100 µM DNA , 3 µL of 2 µM gRNA and 3 µL of 1 µM dsDNA activator and 258 µL of nanopure water. Next, 30 µL of the sample was automatedly injected into reversed-phase HPLC with agilent C18 column (653950-702) and allowed to run at 0.5 mL min^{-1} flow rate on a mobile phase of 0.1 M TEAA : acetonitrile 85:15 v/v, with 0.5% min^{-1} gradient for 28 min, and the corresponding product was identified based on 260 nm

absorption. Immediately after the injection, 3 µL of 1 µM Lba Cas12a solution was added to the same 300 µL vial containing the remaining oligonucleotide mixture. Then, the HPLC was program to inject 30 µL of the solution from this vial after 1, 3, 6, 9, 12, 18 and 24 hour time points. After completion of the injection, the area under corresponding peak was measured using the (Agilent OpenLab CDS software Rev. C.01.10 [287]). Next, the data was normalized relative to the solution without Cas12a enzyme and the data were fitted to a single exponential in GraphPad Prism version 8.4.3 for Windows. To calculate the cleavage rate (k_{obs}), we used the nonlinear curve fitted value from the GraphPad Prism software. PC(t = 0) was set to 0, and PC(t=24) was set to 100%. The data was triplicated, and in each dataset, separated k_{obs} value was calculated and averaged.

Synthesis of tetraPEG DBCO: tPEG DBCO was synthesized using tPEG NH_2 (Mw = 10k g mol^{-1}). First, 10.0 mg of tPEG NH_2 was dissolved in 60 µL of anhydrous DMSO. The solution was mixed with 2.0 mg of DBCO NHS ester in 20 µL of anhydrous DMSO to react for 30 minutes in a dark container. After the reaction, the reaction mixture was added 830 µL of Milli-Q grade water to dilute the mixture for HPLC injection. The resulting mixture was filtered through 0.2 µm centrifugal tubes at 2500*g* for 5 minutes. Then, the reaction mixture was injected into reversed-phase HPLC (Agilent Technologies 1260 Infinity II). For the separation, 30 µL of sample in each time was injected into GL sciences C18 column (5020-07446) and allowed to run at 1.0 mL min^{-1} flow rate on a mobile phase of water : acetonitrile (60:40 v/v with 1.5% min^{-1} gradient for 20 min) and the product was collected based on the characteristic absorption of DBCO at 315 nm. The separated product was lyophilized, and the dry weight of the product (*m*) (≈5.0 mg) was accurately measured using (Mettler Toledo-Analytical Balance MS105). Next, the product with known dry mass was dissolved in a known amount of water (≈ 1.0 mL) and the absorbance at 307 nm (A_{307}) measured by UV-Vis spectrometer was quantified. We used the molar absorption coefficient of DBCO ($\varepsilon_{307\ nm}$ = 12,000 mol^{-1} L cm^{-1}) for the estimation of the DBCO concentration in the product.[38] With the equation 2, we calculated the DOL (x) of DBCO for tPEG molecules. Where, *M* = 10000

gmol^{-1}, A_{307} = observed absorbance of product at 307 nm, v = volume of water added to dissolve the dried product in L and l = path length of the UV-Vis spectrometer. Note that since $x > 0$, we only considered the positive value of x from the quadratic equation.

$$\frac{m}{M+287.3x} = \frac{xvA_{307}}{\varepsilon_{307}l} \qquad (2)$$

Synthesis of bisazide modified DNA: Bisazide modified DNA was synthesized by reacting bisamine modified DNA with azido-PEG$_4$-NHS ester. To a solution of 1.0 mM bisamine modified DNA in 100 µL of milli-Q grade water was added 20 µL of 10X phosphate buffer saline (PBS), 20 µL of 1.0 M freshly prepared $NaHCO_3$, and 250 µL of 10 mg/mL azido-PEG$_4$-NHS ester in DMSO, and the reaction mixture was allowed to react for 30 minutes at room temperature. After the reaction, 520 µL of milli-Q grade water was added to the reaction mixture to quench the reaction. Next, the mixture was filtered using 0.2 µm centrifugal tubes at 2500*g* for 5 minutes. The filtrate was purified by into reverse-phase HPLC column. For the separation 150 µL of sample was injected into agilent C18 column (653950-702) and allowed to run at 0.5 mL min^{-1} flow rate on a mobile phase of 0.1 M TEAA : acetonitrile (for ssDNA, 0% GC HP, and 80% GC HP 85:15 v/v, with 0.5% min^{-1} gradient for 16 min and for 100% GC HP 83:17 v/v, with 0.5% min^{-1} gradient for 20 min), and the product was collected based on 260 nm absorption. The formation of the product was confirmed using high resolution ESI mass spectrometry.

Modified glass slide preparation: 1. 25×75 microscope slides; First, microscope glass slides (Globe Diamond, 25 × 75 mm) were installed in a glass slide rack and washed for 10 minutes with milli-Q grade water, ethanol, and then milli-Q grade water by sonication. Next the glass slides with the rack were carefully introduced into the piranha solution (12mL of H_2O_2 (30%) and 30 mL of conc. H_2SO_4, **CAUTION: piranha is extremely corrosive and may explode if exposed to organics**) and let sit for 30 minutes. Then, glass slides were

thoroughly washed with nanopure water and dried for 3 hours. Next, a solution of dimethyldichlorosilane was added to the 150 mL petri dish and the piranha-etched glass slides were dipped in the solution for 10 minutes. The glass slides were taken out and rinsed with ethanol and then with nanopure water. The surface-modified glass slides were stored in a closed container to avoid attaching dust particles.

2. 25 mm circular coverslips; The coverslips were piranha etched as mentioned in the previous step. Next, one side of the coverslip was treated with dimethyldichlorosilane solution and rinsed with ethanol and then with nanopure water. After that, the glass slides were stored in a closed container to avoid attaching dust particles.

Modified AuNP synthesis: First, 1.0 mL of 100 nm diameter, AuNP solution (OD = 1) was spun down at 2000*g* for 30 minutes. Next 980 µL of the supernatant was pipetted out. Then, 1 mg mL^{-1} solution of PEG-SH (Mw = 5000 g mol^{-1}) milli-Q grade water was added to the AuNP pellets and mixed vigorously. The mixture solution was stored at –80 ºC for 30 minutes to functionalize the AuNPs with PEG molecules. Then, the mixture was spun down at 2000*g* for 30 minutes. Finally, 1.0 mL of the supernatant was pipetted out and the concentration of the AuNP in the solution was measured using the UV-Vis spectrometer.

Optimization of hydrogel volume: The optimization of hydrogel volume was performed as follows. First, hydrogels were synthesized by mixing 4.0 µL of 5.0 mM bisazide PEG crosslinker, 1.0 µL 10X NEB r2.1 buffer, 0.5 µL modified AuNP, and 2.5 µL nanopure water in a PCR tube. Next, 2.0 µL of 5.0 mM tPEG DBCO solution was added to the other solution and mixed by pipetting up and down. Immediately, the solution was transferred on top of a modified glass slide. Note that before the synthesis of the hydrogel, the glass slide was placed inside a petri dish with a filter paper (soaked with nanopure water) at the bottom and placed inside the 37 ºC incubator for 10 minutes (Figure 3(A center)). After the completion of the gelation, 250 µL of 1X NEB r2.1 buffer was added on top of the hydrogel. Next the

formed hydrogel was photographed using smart phone camera to find the initial area (A_i) of the hydrogel using ImageJ software. Then, two 200 µm thick glass slides were placed at both ends of the glass slide as the spacers. Next, using a second modified glass slide the hydrogel was carefully covered and hydrogel was sandwiched with glass slides and applied force using four binding clips (Figure 3(A right corner)). The stretched hydrogel was photographed using smartphone camera to find the final area (A_f) of the hydrogel using ImageJ software. Note that a linear scale was used to calibrate the measured areas of the hydrogels. Using the values of (A_i) and (A_f), the area strain ($\gamma_A(V)$) of the hydrogels was calculated using the equation (3). Finally, the same procedure was repeated for final hydrogel volumes from 20 µL – 60 µL in steps of 10 µL by keeping the concentrations of bisazide PEG and tPEG DBCO constant and plotted as shown in the Figure S10.

$$\gamma_A(V) = \left(\frac{A_f - A_i}{A_i}\right) \times 100 \qquad (3)$$

The average radial strains ($\gamma_R(V)$) were calculated by using the equation (4). Note that here we assumed the hydrogels form circular shapes.

$$\gamma_R(V) = \left(\frac{\sqrt{A_f} - \sqrt{A_i}}{\sqrt{A_i}}\right) \qquad (4)$$

Synthesis of PEG hydrogel crosslinked with bisazide-PEG or bisazide-DNA: In this experiment, we have synthesized two different kinds of hydrogels. First, we have synthesized PEG only hydrogel by crosslinking tPEG DBCO (Mw = 10k g mol^{-1}) and bisazide PEG (Mw = 1k g mol^{-1}). For synthesis of this type of PEG hydrogels, 5.0 mM solutions of tPEG DBCO and bisazide PEG were freshly prepared by dissolving in milli-Q grade water. Then, 12.0 µL of 5.0 mM bisazide PEG was mixed with 3.0 µL of 10X NEB r2.1 buffer and 9.0 µL of milli-Q grade water in a PCR tube. Resulting mixture was then mixed with 6.0 µL of

5.0 mM tPEG DBCO solution, and the final mixture was incubated at 37 ºC for 10 minutes to complete the gelation. By adding 10 µL tip on top of the gel, gelation was confirmed (Figure 2(D)). Next, we synthesized DNA crosslinked PEG hydrogel by crosslinking tPEG DBCO (Mw = 10k g mol^{-1}) and bisazide modified DNA. First, 12.0 µL of 5.0 mM pre-hybridized DNA crosslinker in milli-Q grade water was mixed with 3.0 µL of NEB r2.1 buffer and 9.0 µL of milli-Q grade water in a PCR tube. The resulting mixture was incubated at 37 °C for 10 minutes. The formation of the gel was confirmed by adding 10 µL tip on top of the gel (Figure 2(D)). The hydrogels which contain Cas12a enzyme was synthesized as follows. First, activated Cas12a was prepared by mixing 3.0 µL of 100 µM Lba Cas12a (Cpf1), 3.0 µL of 200 µM gRNA, 1.0 µL of 10X NEB r2.1 buffer and 3.0 µL of nanopure water in a PCR tube, and then this mixture was incubated at 37 °C for 5 minutes. In a separate PCR tube, 12.0 µL of 5.0 mM pre-hybridized DNA crosslinker was mixed with 2.0 µL of 10X NEB r2.1 buffer, 3.0 µL of 100 µM dsDNA activator, 1.0 µL of modified AuNP (~3.8×10^{11} particles mL^{-1}) and 6.0 µL of activated Cas12a solution were mixed in a PCR tube. Next, 6.0 µL of 5.0 mM tPEG DBCO solution was added to the mixture and pipetted to mix uniformly. Then, the solution mixture was incubated at 37 ºC for 10 minutes to complete the gelation.

Electron Spray Ionization (ESI) Mass Spectrometry: The molecular weight of the products was evaluated with an electron spray ionization (ESI) method using a Thermo Fisher Scientific Orbitrap. The oligo samples were prepared in the mixture of 70% 18.2 MΩ MilliQ water and 30% methanol containing 10 µM ethylenediaminetetraacetic acid (EDTA), 0.0375% triethylamine, and 0.75% of 1,1,1,3,3,3-hexafluoro-2-propanol (HFIP) and recorded the spectra with negative charge mode eluted with 60% water/ 40% methanol mixture.[39] The obtained ESI-MS spectrum (*m/z*) was then deconvoluted for the main peak to obtain average molecular weight for the oligonucleotides.

Force-triggered self-destruction with glass coverslip: Force-triggered self-destruction of the DNA crosslinked hydrogel was tested for two conditions without and with external force. For the control experiment of self-destruction without external force, each hydrogel precursor

solution with activated Cas12a was mixed in a PCR tube as mentioned in the previous paragraph. Immediately after the mixing, the solution was transferred on top of a modified glass slide (Figure 3(A center)). Next, as mentioned above, the solution was incubated inside a closed petri dish with 100% humidity inside the incubator at 37 ºC for 10 minutes to complete the gelation. Then, 250 µL of 1X NEB r2.1 buffer was pipetted on top of the hydrogel. Next, the hydrogel was incubated at 37 ºC to evaluate the self-destruction. After 3 hours of incubation, 200 µL of buffer was pipetted out from the buffer after few times of pipetting up and down to mix the solution uniformly. Next, the pipetted solution was centrifuged 2000*g* for 15 minutes at room temperature, and 190 µL of the supernatant was carefully pipetted out from the solution by not disturbing the particle pellet at the bottom. Next, the pellet was mixed uniformly by pipetting up and down and the absorbance at 535 nm was measured using UV-Vis spectrometer. This absorbance value was noted as the OD @ λ = 535 nm (Figure 3(C)).

For the self-destruction with the external force, the hydrogel was prepared as described above. Then, the external force was applied as shown in the Figure 3(A right center) and incubated at 37 ºC for 3 hours. After the incubation, the sandwiched hydrogel with two glass slides were taken out and top glass slide was carefully removed. Next, AuNP release was measured as mentioned in the above paragraph. Force-triggered self-destruction of the hydrogel under lower Cas12a enzyme concentration was measure using the same method, but the activated Cas12a solution was prepared using 10X lower concentrations of Cas12a and gRNA in 10X NEB r2.1 buffer. Also, the used activator dsDNA solution was a 10 µM concentration.

External addition of Cas12a to hydrogel: Force-triggered hydrogel degradation when the Cas12a enzyme was introduced externally was tested as follows. First, the hydrogel was synthesized on a modified glass slide using 12.0 µL of 5.0 mM pre-hybridized DNA crosslinker, 3.0 µL of 10X NEB r2.1 buffer, 3.0 µL of 100 µM dsDNA activator, 1.0 µL of

modified AuNP (~3.8 × 10^{11} particles mL^{-1}) and 6.0 µL of 5.0 mM tPEG DBCO. Then, 1X NEB r2.1 buffer solution with activated Cas12a was prepared by mixing 20 µL solution of activated Cas12a and 130 µL solution of 1X NEB r2.1 buffer solution. Next, this solution mixture was added on top of the synthesized hydrogel and the hydrogel degradation with/without external force was tested as mentioned previously.

Standard rheology experiment: Hydrogel formation was confirmed with rheology. Rheological measurements were performed using 25 mm steel parallel plates. First, to identify the gelation kinetics, 30 µL of precursors to synthesize DNA crosslinked hydrogel was mixed in a PCR tube as mentioned in prior section (bisazide crosslinkers and tPEG DBCO). Immediately after mixing, the solution was loaded into the rheometer, and time sweep experiment was performed at 1% strain and 1 Hz frequency for 50 minutes at 37 ºC. Note that the gap size was set to 50 µm. Next, immediately after the time sweep experiment, the same hydrogel sample was used to carry out the frequency sweep experiments, in which the frequencies were ranging from 0.01 Hz to 100 Hz at 37 ºC at a fixed strain of 1%.

Force-triggered self-destruction with rheology: Force-triggered self-destruction of the hydrogels was tested as follows (Figure S13A). First, a modified coverslip was attached to the top plate (25 mm) of the rheometer using double sided adhesive tape. Note that the unmodified side of the coverslip was attached to the rheometer plate. Next, a modified (25×75 mm) glass slide was attached to the bottom plate of the rheometer using double sided adhesive tape (make sure this glass slide is aligned with the top plate). Next, the gap between upper and lower plates were zeroed. Introducing the hydrophobic glass coverslip in rheology machine is crucial for our measurement as it maintains the droplet structure of the hydrogel. To confirm these glass coverslips do not alter the rheology measurement, we measured a standard PDMS polymer with and without a glass coverslip (Figure S17). This result confirmed our expectation that glass coverslip introduction does not significantly alter the rheology measurement when the force is applied in a perpendicular orientation.

For the force-triggered self-destruction, 30 µL hydrogels were synthesized by mixing 12 µL of 5.0 mM DNA crosslinker, 3.0 µL dsDNA activator, 2 µL of 10X NEB r2.1 buffer, 6 µL of activated Cas12a and 6 µL of 5.0 mM tPEG DBCO in a PCR tube. Next the mixture was immediately loaded on top of the 25×75 mm glass slide on the rheometer. Note that before loading the hydrogel on top of the rheometer plate it was heated to 37 ºC. After 10 minutes wait time for the gelation, the squeeze experiment was run to measure the time-dependent applied force using the 10 µm s^{-1} pushing speed until the gap size is equal to 200 µm. Immediately after pushing the two plates to a distance of 200 µm, the stress relaxation of the hydrogel was measured as a function of time. For the comparison of the hydrogel stress relaxations, we normalized the normal force on the hydrogels to the maximum normal force applied on the each hydrogel.

References

[1] a)D. Wang, J. Duan, J. Liu, H. Yi, Z. Zhang, H. Song, Y. Li, K. Zhang, *Adv. Healthcare Mater.* **2023**, 12, 2203031; b)Q. Zhang, N. Re Ko, J. Kwon Oh, *Chem. Commun.* **2012**, 48, 7542; c)V. Delplace, J. Nicolas, *Nat. Chem.* **2015**, 7, 771.

[2] H. Tanaka, T. Takahashi, M. Konishi, N. Takata, M. Gomi, D. Shirane, R. Miyama, S. Hagiwara, Y. Yamasaki, Y. Sakurai, K. Ueda, K. Higashi, K. Moribe, E. Shinsho, R. Nishida, K. Fukuzawa, E. Yonemochi, K. Okuwaki, Y. Mochizuki, Y. Nakai, K. Tange, H. Yoshioka, S. Tamagawa, H. Akita, *Adv. Funct. Mater.* **2020**, 30, 1910575.

[3] a)T. Yoshida, T. C. Lai, G. S. Kwon, K. Sako, *Expert Opin. Drug Deliv.* **2013**, 10, 1497; b)A. H. Agergaard, A. Sommerfeldt, S. U. Pedersen, H. Birkedal, K. Daasbjerg, *Angew. Chem. Int. Ed.* **2021**, 60, 21543; c)H. Liu, Z. Hu, H. Chen, Y. Yan, Z. Le, C. Wei, W. Cao, T. Chen, Y. Chen, L. Liu, *J. Control. Release* **2022**, 345, 91; d)M. Mizutani, E. F. Palermo, L. M. Thoma, K. Satoh, M. Kamigaito, K. Kuroda, *Biomacromolecules* **2012**, 13, 1554.

[4] C. M. Geiselhart, W. Xue, C. Barner-Kowollik, H. Mutlu, *Macromolecules* **2021**, 54, 1775.

[5] a)G. Liu, X. Wang, J. Hu, G. Zhang, S. Liu, *J. Am. Chem. Soc.* **2014**, 136, 7492; b)K. Barker, S. K. Rastogi, J. Dominguez, T. Cantu, W. Brittain, J. Irvin, T. Betancourt, *J. Biomater. Sci. Polym. Ed.* **2016**,

27, 22; c)Q. Zhu, X. Chen, X. Xu, Y. Zhang, C. Zhang, R. Mo, *Adv. Funct. Mater.* **2018**, 28, 1707371; d)Q. Huang, S. Kimura, T. Iwata, *Polym. Degrad. Stab.* **2021**, 190, 109647.

[6] a)W. Seo, S. T. Phillips, *J. Am. Chem. Soc.* **2010**, 132, 9234; b)Y. Xiao, H. Li, B. Zhang, Z. Cheng, Y. Li, X. Tan, K. Zhang, *Macromolecules* **2018**, 51, 2899.

[7] a)B. Huang, M. Wei, E. Vargo, Y. Qian, T. Xu, F. D. Toste, *J. Am. Chem. Soc.* **2021**, 143, 17920; b)H. Huang, W. Xie, Q. Wan, L. Mao, D. Hu, H. Sun, X. Zhang, Y. Wei, *Adv. Sci.* **2022**, 9, 2104101.

[8] X. Meng, M. Gao, J. Deng, D. Lu, A. Fan, D. Ding, D. Kong, Z. Wang, Y. Zhao, *Nano Res.* **2018**, 11, 6177.

[9] D.-H. Lee, S. A. Valenzuela, M. N. Dominguez, M. Otsuka, D. J. Milliron, E. V. Anslyn, *Cell Rep. Phys. Sci.* **2021**, 2, 100552.

[10] a)Y. Xiao, X. Tan, Z. Li, K. Zhang, *J. Mater. Chem. B* **2020**, 8, 6697; b)C. Ergene, E. F. Palermo, *Biomacromolecules* **2017**, 18, 3400; c)C. Ergene, K. Yasuhara, E. F. Palermo, *Polym. Chem.* **2018**, 9, 2407; d)M. A. DeWit, E. R. Gillies, *J. Am. Chem. Soc.* **2009**, 131, 18327.

[11] a)R. Petrosyan, A. Narayan, M. T. Woodside, *J. Mol. Biol.* **2021**, 433, 167207; b)C. M. Madl, L. M. Katz, S. C. Heilshorn, *Adv. Funct. Mater.* **2016**, 26, 3612.

[12] A. del Rio, R. Perez-Jimenez, R. Liu, P. Roca-Cusachs, J. M. Fernandez, M. P. Sheetz, *Science* **2009**, 323, 638.

[13] Y. Zhang, J. Yu, H. N. Bomba, Y. Zhu, Z. Gu, *Chem. Rev.* **2016**, 116, 12536.

[14] T. Friščić, C. Mottillo, H. M. Titi, *Angew. Chem., Int. Ed.* **2020**, 59, 1018.

[15] a)Y. Chen, G. Mellot, D. van Luijk, C. Creton, R. P. Sijbesma, *Chem. Soc. Rev.* **2021**, 50, 4100; b)M. K. Beyer, H. Clausen-Schaumann, *Chem. Rev.* **2005**, 105, 2921.

[16] S. Garcia-Manyes, A. E. M. Beedle, *Nat. Rev. Chem.* **2017**, 1, 0083.

[17] a)A. S. Hoffman, *Adv. Drug Deliv. Rev.* **2012**, 64, 18; b)R. Narayanaswamy, V. P. Torchilin, *Molecules* **2019**, 24, 603; c)Y. Dong, A. N. Ramey-Ward, K. Salaita, *Adv. Mater.* **2021**, 33, 2006600; d)M. E. Allen, J. W. Hindley, D. K. Baxani, O. Ces, Y. Elani, *Nat. Rev. Chem.* **2022**, 6, 562.

[18] a)M. T. Woodside, W. M. Behnke-Parks, K. Larizadeh, K. Travers, D. Herschlag, S. M. Block, *Proc. Natl. Acad. Sci. U. S. A.* **2006**, 103, 6190; b)K. Hatch, C. Danilowicz, V. Coljee, M. Prentiss, *Phys. Rev. E* . **2008**, 78, 011920.

[19] a)M. A. English, L. R. Soenksen, R. V. Gayet, H. de Puig, N. M. Angenent-Mari, A. S. Mao, P. Q. Nguyen, J. J. Collins, *Science* **2019**, 365, 780; b)X. Gao, X. Li, X. Sun, J. Zhang, Y. Zhao, X. Liu, F. Li,

Anal. Chem. **2020**, 92, 4592; c)C. Yao, H. Tang, W. Wu, J. Tang, W. Guo, D. Luo, D. Yang, *J. Am. Chem. Soc.* **2020**, 142, 3422.

[20] J. Gačanin, C. V. Synatschke, T. Weil, *Adv. Funct. Mater.* **2020**, 30, 1906253.

[21] a)Y. Zhang, C. Ge, C. Zhu, K. Salaita, *Nat. Commun.* **2014**, 5, 5167; b)Y. Liu, L. Blanchfield, V. P.-Y. Ma, R. Andargachew, K. Galior, Z. Liu, B. Evavold, K. Salaita, *Proc. Natl. Acad. Sci. U. S. A.* **2016**, 113, 5610; c)Y. Zhang, Y. Qiu, A. T. Blanchard, Y. Chang, J. M. Brockman, V. P. Ma, W. A. Lam, K. Salaita, *Proc. Natl. Acad. Sci. U. S. A.* **2018**, 115, 325.

[22] a)G. Creusen, R. S. Schmidt, A. Walther, *ACS Macro Lett.* **2021**, 10, 671; b)R. Merindol, G. Delechiave, L. Heinen, L. H. Catalani, A. Walther, *Nat. Commun.* **2019**, 10, 528.

[23] J. S. Chen, E. Ma, L. B. Harrington, M. Da Costa, X. Tian, J. M. Palefsky, J. A. Doudna, *Science* **2018**, 360, 436.

[24] D. Guillen, M. Schievelbein, K. Patel, D. Jose, J. Ouellet, *PLoS One* **2020**, 15, e0229527.

[25] M. Rossetti, R. Merlo, N. Bagheri, D. Moscone, A. Valenti, A. Saha, Pablo R. Arantes, R. Ippodrino, F. Ricci, I. Treglia, E. Delibato, J. van der Oost, G. Palermo, G. Perugino, A. Porchetta, *Nucleic Acids Res.* **2022**, 50, 8377.

[26] T. Sakai, T. Matsunaga, Y. Yamamoto, C. Ito, R. Yoshida, S. Suzuki, N. Sasaki, M. Shibayama, U.-i. Chung, *Macromolecules* **2008**, 41, 5379.

[27] a)M. Ohira, T. Katashima, M. Naito, D. Aoki, Y. Yoshikawa, H. Iwase, S.-i. Takata, K. Miyata, U.-i. Chung, T. Sakai, M. Shibayama, X. Li, *Adv. Mater.* **2022**, 34, 2108818; b)C. O. Akintayo, G. Creusen, P. Straub, A. Walther, *Macromolecules* **2021**, 54, 7125; c)K. Barker, S. K. Rastogi, J. Dominguez, T. Cantu, W. Brittain, J. Irvin, T. Betancourt, *J. Biomater. Sci., Polym. Ed.* **2016**, 27, 22.

[28] H. Zhan, H. de Jong, D. W. P. M. Löwik, *ACS Appl. Bio Mater.* **2019**, 2, 2862.

[29] S. T. Lust, D. Hoogland, M. D. A. Norman, C. Kerins, J. Omar, G. M. Jowett, T. T. L. Yu, Z. Yan, J. Z. Xu, D. Marciano, R. M. P. da Silva, C. A. Dreiss, P. Lamata, R. J. Shipley, E. Gentleman, *ACS Biomater. Sci. Eng.* **2021**, 7, 4293.

[30] G. Altan-Bonnet, A. Libchaber, O. Krichevsky, *Phys. Rev. Lett.* **2003**, 90, 138101.

[31] H. Su, J. M. Brockman, Y. Duan, N. Sen, H. Chhabra, A. Bazrafshan, A. T. Blanchard, T. Meyer, B. Andrews, J. P. K. Doye, Y. Ke, R. B. Dyer, K. Salaita, *J. Am. Chem. Soc.* **2021**, 143, 19466.

[32] B. Paul, L. Chaubet, D. E. Verver, G. Montoya, *Nucleic Acids Res.* **2021**, 50, 5208.

[33] T. Yamano, H. Nishimasu, B. Zetsche, H. Hirano, I. M. Slaymaker, Y. Li, I. Fedorova, T. Nakane, K. S. Makarova, E. V. Koonin, R. Ishitani, F. Zhang, O. Nureki, *Cell* **2016**, 165, 949.

[34] a)Y. Hu, X. Zhao, J. J. Vlassak, Z. Suo, *Appl. Phys. Lett.* **2010**, 96, 121904; b)J. D. Berry, M. Biviano, R. R. Dagastine, *Soft Matter* **2020**, 16, 5314; c)J.-F. Louf, S. S. Datta, *Soft Matter* **2021**, 17, 3840; d)J. Hazur, N. Endrizzi, D. W. Schubert, A. R. Boccaccini, B. Fabry, *Biomater. Sci.* **2022**, 10, 270.

[35] a)D. A. Giljohann, D. S. Seferos, W. L. Daniel, M. D. Massich, P. C. Patel, C. A. Mirkin, *Angew. Chem. Int. Ed.* **2010**, 49, 3280; b)Y. Jiang, N. Krishnan, J. Heo, R. H. Fang, L. Zhang, *J. Control. Release* **2020**, 324, 505; c)S. Merino, C. Martín, K. Kostarelos, M. Prato, E. Vázquez, *ACS Nano* **2015**, 9, 4686.

[36] a)A. Stejskalová, N. Oliva, F. J. England, B. D. Almquist, *Adv. Mater.* **2019**, 31, 1806380; b)Y. Wang, A. V. Pisapati, X. F. Zhang, X. Cheng, *Adv. Healthc. Mater.* **2021**, 10, e2002196.

[37] Wetterstrand KA. DNA Sequencing Costs: Data from the NHGRI Genome Sequencing Program (GSP) Available at: www.genome.gov/sequencingcostsdata. Accessed [August 10th 2023].

[38] N. Kotagiri, Z. Li, X. Xu, S. Mondal, A. Nehorai, S. Achilefu, *Bioconjug. Chem.* **2014**, 25, 1272.

[39] M. E. Hail, B. Elliott, K. Anderson, *Am. Biotechnol. Lab.* **2004**, 12, 12.

Table of Content

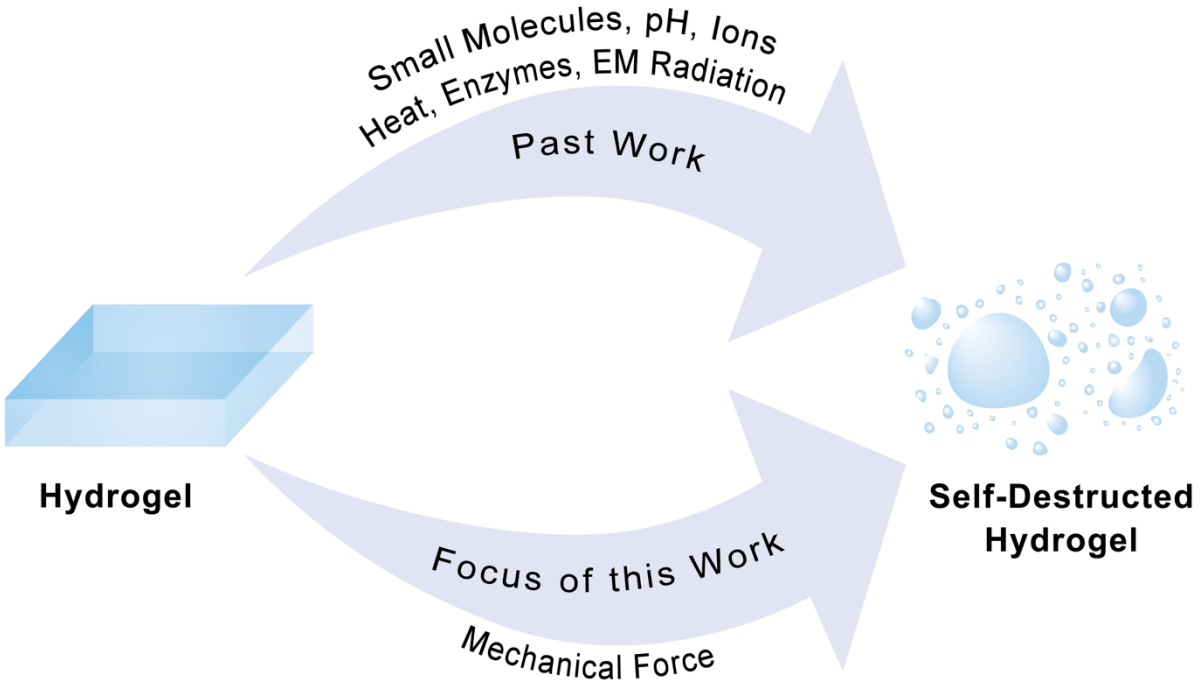

Force-triggered self-destructive hydrogels were developed by using mechano-responsive DNA hairpins and selectively cleaved upon unfolding. The DNA is protected by folding without force, but under force, cryptic sites are exposed which allows Cas12a nuclease to destroy the phosphodiester DNA backbone. Here we demonstrate tunable force sensitivity to trigger self-destruction and cargo release from the hydrogel.